Catalysis Today 158 (2010) 470–474

Contents lists available at ScienceDirect

Catalysis Today

journal homepage: www.elsevier.com/locate/cattod

Effect of ZrO_2 promoter on structure and catalytic activity of the Ni/SiO_2 catalyst for CO methanation in hydrogen-rich gases

Yongzhao Wang, Ruifang Wu, Yongxiang Zhao*

School of Chemistry and Chemical Engineering, Engineering Research Center of Ministry of Education for Fine Chemicals, Shanxi University, Wucheng Road No. 92, Shanxi, Taiyuan 030006, PR China

ARTICLE INFO

Keywords:
Ni/SiO_2
$Ni/ZrO_2–SiO_2$
Promoter
CO methanation

ABSTRACT

Ni-based catalysts supported on SiO_2 aerogel that is unpromoted (Ni/SiO_2) or promoted ($Ni/ZrO_2–SiO_2$) with ZrO_2 are prepared by the incipient-wetness impregnation method. Their catalytic activities for CO methanation in hydrogen-rich gases with 1 vol.% CO are studied with a continuous flowing microreactor. It is found that the $Ni/ZrO_2–SiO_2$ catalyst shows higher catalytic activity, over which CO can be completely converted into CH_4 at 240 °C. However, CO cannot be completely converted until the temperature was raised to 320 °C over the Ni/SiO_2 catalyst under the same reaction conditions. Characterizations using FT-IR, XRD, TEM, NH_3-TPD, H_2-TPR and H_2-TPD suggest that the formation of Si–O–Zr bond results in stronger acid strength and larger amounts of acid of the $ZrO_2–SiO_2$ support. The changes of acidity lead to the increase of the interaction between NiO species and the $ZrO_2–SiO_2$ support and then enhance the dispersion degree and the reduction degree of NiO species. Thus, the $Ni/ZrO_2–SiO_2$ catalyst possesses smaller Ni crystallite size, higher Ni dispersion, more active Ni species and stronger adsorption ability for H_2, which may contribute to its higher catalytic activity for CO methanation.

1. Introduction

Hydrogen has been widely used as a fuel for proton exchange membrane fuel cells (PEMFCs) because of its high conversion efficiency of the chemical energy into electricity without emission of any pollutant gases [1–3]. At present, most hydrogen is produced through steam reforming and partial oxidation of methane or methanol [4], however, 1–2 vol.% CO is inevitably co-produced in these reactions, which can poison the Pt anodes and decrease the efficiency of the PEMFCs greatly [5]. Thus, in order to avoid poisoning fuel cell electrodes CO concentration in hydrogen-rich gases must be reduced catalytically to less than 10 ppm [6]. Among the methods of the removal of CO, methanation has been proved to be an effective strategy, because the method is somewhat simple and does not require adding the necessary reactants (CO and H_2) that are already present [7].

Among these studies, the investigation of Ni-based catalysts for CO methanation was the most active [8]. The commonly used supports include α- or γ-Al_2O_3, kaolin and calcium aluminate cement, and the promoters include alkali metal Na, alkaline-earth metal Mg, rare earth metals and so on. SiO_2 aerogel has been widely used as a support because of its advantages such as small particle size, high specific surface area and high porosity [9–12]. ZrO_2 has also been widely used as a promoter due to its redox and acid–base properties [13–15]. Li et al. [13] reported that the addition of ZrO_2 promoter in CuZnAlO catalyst could increase the conversion of methanol and selectivity of H_2 in the methanol steam reforming reaction. The addition of ZrO_2 promoter could inhibit the deactivation of Co/SiO_2 catalyst and improve its stability for F–T synthesis that had been reported by Zhou et al. [14]. Rana et al. [15] also found that incorporation of ZrO_2 with SiO_2 strengthened the weak interaction of active phases with SiO_2 support, overcame poor dispersion on the support surface, and therefore efficiently improved the activity of the $MoCo(Ni)/ZrO_2–SiO_2$ catalyst through enhanced number of active sites as well as activity per site. However, to our knowledge Ni-based catalysts supported on SiO_2 aerogel promoted by ZrO_2 are studied less for CO methanation.

In this work, the Ni/SiO_2 and $Ni/ZrO_2–SiO_2$ catalysts were prepared by the incipient-wetness impregnation method using SiO_2 aerogel support unprompted or promoted with ZrO_2. Their catalytic activities and the effect of ZrO_2 promoter on structure and catalytic activity of the Ni/SiO_2 catalyst for CO methanation were investigated. Combined with characterizations, a possible reason for higher catalytic activity of the $Ni/ZrO_2–SiO_2$ catalyst has been given.

* Corresponding author. Tel.: +86 351 7011587; fax: +86 351 7011688.
E-mail address: yxzhao@sxu.edu.cn (Y. Zhao).

0920-5861/$ – see front matter © 2010 Elsevier B.V. All rights reserved.
doi:10.1016/j.cattod.2010.07.016

2. Experimental

2.1. Catalyst preparation

The SiO_2 aerogel support promoted with ZrO_2 was prepared according to our previous work [16]. The following is a typical preparation procedure: the desired amounts of zirconyl nitrate dihydrate ($ZrO(NO_3)_2{\cdot}2H_2O$) was dissolved in anhydrous ethanol at room temperature. Then acetic acid, water and tetraethoxysilicane (TEOS) were added with constant stirring. The above mixture was dried in a stainless-steel tank via the supercritical drying. In order to exceed the critical condition without a formation of vapor–liquid interface inside the pores, the mixture was transferred into a stainless-steel liner in an autoclave. By being heated, the temperature and pressure of the liquid in the autoclave could surpass the T_c (243 °C) and P_c (6.36 MPa) of ethanol. The final temperature and pressure were about 270 °C and 8.0 MPa, respectively. The autoclave was kept at the final temperature for 30 min to ensure complete thermal equilibration. Then the fluid was released and flushed with nitrogen to cool down to room temperature. The SiO_2 aerogel support promoted with 10 wt%ZrO_2 was obtained. The ZrO_2 content 10 wt% was selected in this work according to a content selection test (data not shown). The SiO_2 aerogel unpromoted with ZrO_2 was prepared with the same above process without adding $ZrO(NO_3)_2{\cdot}2H_2O$.

The Ni/SiO_2 and Ni/ZrO_2–SiO_2 catalysts were prepared by impregnating the above supports with an aqueous solution of $Ni(NO_3)_2{\cdot}6H_2O$ with stirring, followed by being dried at 80 °C for 3 h, and then at 120 °C for 3 h, calcined in air at 400 °C for 3 h and reduced with H_2 at 400 °C for 3 h, respectively. The two catalysts obtained were 13 wt%Ni/SiO_2 and 13 wt%Ni/10 wt%ZrO_2–SiO_2, which were labeled as Ni/Si and Ni/Zr–Si, respectively.

2.2. Catalyst characterization

N_2 adsorption–desorption isotherms were measured at −196 °C using Micrometritics ASAP 2020 specific surface area and porosity analyzer. The specific surface area (S_{BET}) was determined from the N_2 adsorption isotherm. The pore structure parameters were obtained from adsorption branch of N_2 with a cylindrical pore model, according to the BJH model. Prior to the adsorption experiments, the samples were degassed under vacuum at 150 °C for 12 h.

Fourier transform infrared (FT-IR) spectra of the samples were obtained with a Bruker TENSOR 27 spectrometer in the range of 400–2000 cm^{-1}. 1 mg of each powder sample was diluted with 100 mg of vacuum-dried IR-grade KBr.

X-ray diffraction (XRD) measurements were performed using a Rigaku D/MAX-2250 X-ray diffractometer with a target of Cu Kα operated at 40 kV and 100 mA with a scanning speed of 6°/min and a scanning angle (2θ) range of 10–80°. Average crystallite size of the samples was evaluated from X-ray line broadening analysis (XLBA) using the well-known Scherrer equation ($d = 0.89\lambda/\beta\cos\theta$) [17].

Transmission electron microscopy (TEM) measurements were carried out using JEM-2100 model TEM operated at 200 kV. Samples for TEM were dispersed by ultrasonic in ethanol followed by deposition of the suspension onto a standard Cu grid covered with a holey carbon film.

NH_3 temperature programmed desorption (NH_3-TPD) experiments were carried out in a tubular quartz reactor. In order to remove surface contaminants 100 mg of sample (40–60 mesh) was pretreated in a flowing N_2 at 500 °C for 2 h, and then cooled down to 50 °C. At this temperature, the flow was switched to He (99.999%) and then 0.5 mL NH_3 pluses were supplied to the samples until no further uptake of ammonia was observed. The temperature was elevated at a heating rate of 15 °C min^{-1} with a flow rate of 60 mL min^{-1}. The desorbed NH_3 was detected using a thermal conductivity detector (TCD).

H_2 temperature programmed reduction (H_2-TPR) experiments were carried out in a tubular quartz reactor, where 30 mg of sample (40–60 mesh) was loaded in the thermostatic zone. The reduction was conducted in a flow of H_2/N_2 mixture (volume ratio, 5:95) with a flow rate of 20 mL min^{-1} and a heating rate of 10 °C min^{-1}. The consumption of H_2 was detected using a TCD.

H_2 temperature programmed desorption (H_2-TPD) experiments were also carried out in the same system as described in TPR experiments. 100 mg of sample (40–60 mesh) was reduced in situ in a flowing H_2 for 3 h at 400 °C, and then swept with Ar (99.999%) for 1 h to yield clean surface. Then, the sample was cooled down to 50 °C and H_2 was adsorbed for 2 h or not. After that the sample was swept with Ar until the gas chromatograph baseline became stable. Finally, the temperature was elevated at a heating rate of 10 °C min^{-1} with a flow rate of 20 mL min^{-1}. The TCD signals of desorbed H_2 were obtained on the basis of the excess of TCD signals measured for the samples adsorbing H_2 with respect to the ones without adsorbing H_2. The TCD area was calibrated by running TPR experiment on a standard Ag_2O sample. Ni dispersion (D) was calculated from the volume of H_2 chemisorbed using the following simplified equations: $D\ (\%) = (V_{ad}FW_{Ni}SF/W_sF_{Ni}V_m) \times 100$, where V_{ad} = volume of H_2 chemisorbed at STP (mL) to form a monolayer, W_s = weight of the sample (g), V_m = molar volume of H_2 gas (22,414 mL mol^{-1}), SF = stoichiometric factor, i.e. Ni:H ratio in the chemisorption, which is taken as 1, F_{Ni} = weight fraction of Ni in the sample, FW_{Ni} = formula weight of Ni (58.71 g mol^{-1}).

2.3. Apparatus and method for activity test

The measurements of catalytic activity for CO methanation were carried out with a continuous flowing laboratory microreactor under atmospheric pressure. The microreactor was 4 mm i.d. quartz u-tube, and a thermocouple was set into the catalyst bed to measure the temperature. The samples were sieved to 40–60 mesh so that concentration and temperature gradients and pressure drop over the catalyst bed were negligible. About 100 mg of catalyst was used for each run. The feed gas, consisted of 1 vol.% CO and 99 vol.% H_2, passed through the catalyst bed with a total flow rate of 60 mL min^{-1}. Quantitative analysis of CO and CH_4 was performed with an on-line gas chromatograph equipped with a 3 m column packed with carbon molecular sieve, a methanator and a flame ionization detector (FID). The minimum detection level was *ca.* 10 ppm. Prior to all catalytic experiments the catalysts were pretreated in flowing H_2 at 400 °C for 1 h to yield clean surface and then cooled in the presence of flowing H_2. The reaction temperature was controlled by the temperature controller and ranged in the range of 100–400 °C at a heating rate of 2 °C min^{-1}.

3. Results and discussion

3.1. Characterization of catalysts

The N_2 adsorption–desorption isotherm analysis results of the Ni/Si and Ni/Zr–Si catalysts are listed in Table 1. Seen obviously from Table 1, the addition of ZrO_2 promoter slightly decreases the

Table 1
S_{BET}, pore volume, average pore size of the catalysts.

Catalyst	S_{BET} ($m^2\ g^{-1}$)	Pore volume ($cm^3\ g^{-1}$)	Average pore size (nm)
Ni/Si	567	0.29	2.63
Ni/Zr–Si	553	0.27	2.59

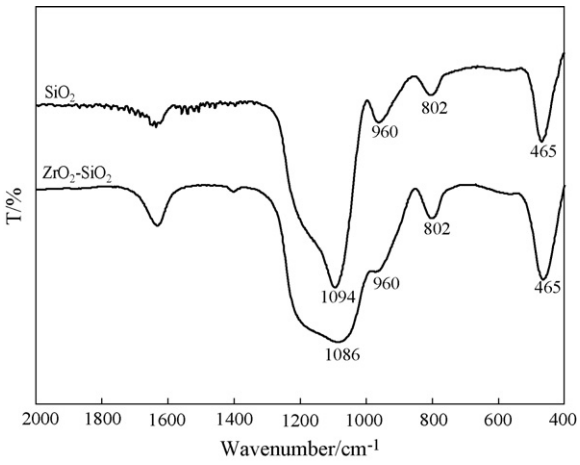

Fig. 1. FT-IR spectra of the SiO_2 and ZrO_2–SiO_2 supports.

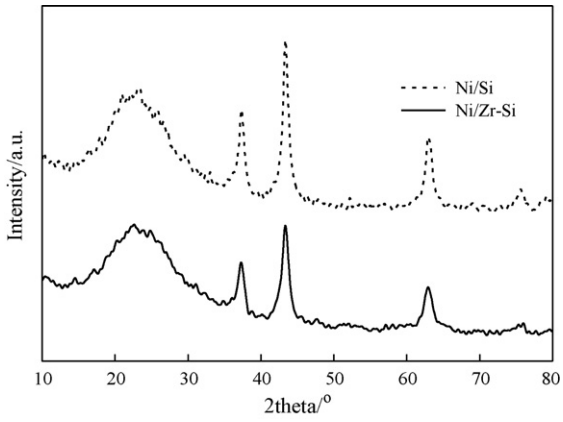

Fig. 2. XRD patterns of the Ni/Si and Ni/Zr–Si catalysts.

S_{BET} (567–553 $m^2\,g^{-1}$), and has little or no influence on the pore structure.

Fig. 1 shows the FT-IR spectra of the SiO_2 and ZrO_2–SiO_2 supports. SiO_2 support is known to exhibit the peak at 1094 cm^{-1} due to the asymmetric stretching vibration, and the peak at 802 cm^{-1} assigned to symmetric stretching vibration of three dimensional Si–O–Si bonds. The peak at 960 cm^{-1}, characteristic of the Si–OH vibration, is also observed. The peak at 465 cm^{-1} corresponds to the bending vibration of the Si–O bonds in a ring structure [18]. The substitutional insertion of the cations into the silica network, which resulted in the weakening of the framework can be easily detected by the wavenumber shift and intensity changes of these peaks. But the mechanical mixtures would give spectra that can be derived by linear combination of the spectra of the components (not shown).

Compared with the SiO_2 support, the asymmetric stretching vibration of the Si–O–Si bond shifts to lower wavenumber, reading as low as 1086 cm^{-1}, and the vibration intensity of the Si–OH bond at 960 cm^{-1} decreases for the ZrO_2–SiO_2 support. Similar observations were reported earlier by Zhan and Zeng [19] and Lee and Condrate [20], which indicates a high incorporation of ZrO_2 in the silica network and the presence of Si–O–Zr bond in the ZrO_2–SiO_2 support.

The XRD patterns of the Ni/Si and Ni/Zr–Si catalysts are presented in Fig. 2. The characteristic peaks ($2\theta = 37.30^\circ, 43.43^\circ, 62.80^\circ$) attributed to cubic NiO and amorphous silica ($2\theta = 22.10^\circ$) are observed in the both samples. But the characteristic peaks of ZrO_2 are not observed in the XRD pattern of the Ni/Zr–Si catalyst. Miller and Ko [21] suggested that the absence of XRD patterns for multicomponent system was the result of high degree mixing of multicomponent oxides. The absence of XRD pattern for ZrO_2 may be due to the incorporation of zirconium atoms in the framework of amorphous SiO_2 and the formation of Si–O–Zr bond, which is in accord with the results of FT-IR.

In addition, it is observed that the characteristic NiO peaks decrease in intensity and is somewhat broad. The average crystallite size of NiO species in the Ni/Si and Ni/Zr–Si catalysts is 18 and 13 nm, respectively, calculated using the Scherrer equation. Apparently, the addition of ZrO_2 promoter enhances the dispersion degree of NiO species in the Ni/Zr–Si catalyst, which is generally consistent with our TEM observation (will be presented shortly).

It is obvious that the TEM image of the Ni/Si catalyst in Fig. 3 shows NiO crystallites are not well distributed on SiO_2 support and a slight aggregation can be observed. But the homogeneous distribution and high dispersion of NiO species on ZrO_2–SiO_2 support can be observed from the TEM image of the Ni/Zr–Si catalyst. The crystallite size of NiO species in the Ni/Si and Ni/Zr–Si catalysts estimated from TEM image is 15–20 and 10–15 nm, respectively, which is generally consistent with the calculation from the broadening of powder diffraction peaks in X-ray patterns. Apparently, NiO species in the Ni/Zr–Si catalyst possesses higher dispersion degree due to the addition of ZrO_2 promoter.

Fig. 4 shows the NH_3-TPD profiles of the SiO_2 and ZrO_2–SiO_2 supports. For the SiO_2 support, there is only a sharp and Gaussian symmetric desorption peak ($T_{max} = 135\,^\circ C$) caused by Si–OH of the support surface, the lower desorption temperature of which suggests weaker acidity. Compared with the SiO_2 support, the low-temperature desorption peak shifts to a higher temperature ($T_{max} = 154\,^\circ C$) for the ZrO_2–SiO_2 support, suggesting that the weak acid strength is enhanced. In addition, another desorption peak also appears in the range of 200–350 °C and total peak area increases obviously, which suggest the existence of medium strong acid sites and increase of the total amounts of acid of the ZrO_2–SiO_2 support.

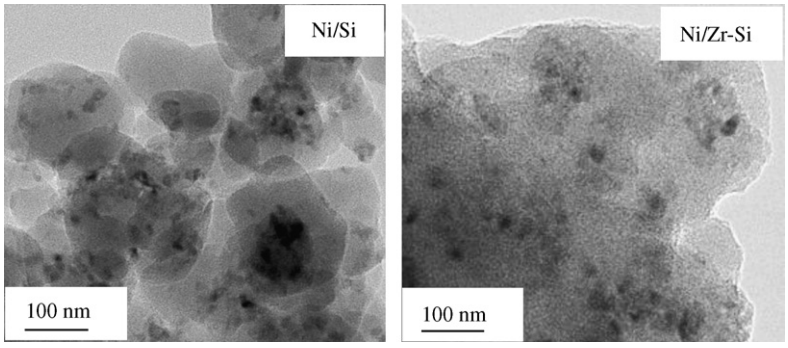

Fig. 3. TEM images of the Ni/Si and Ni/Zr–Si catalysts.

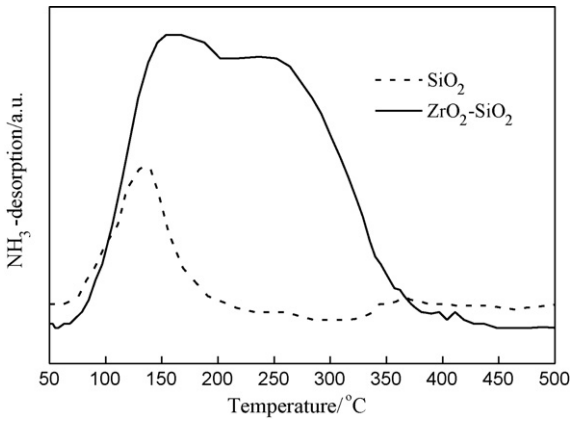

Fig. 4. NH_3-TPD profiles of the SiO_2 and ZrO_2–SiO_2 supports.

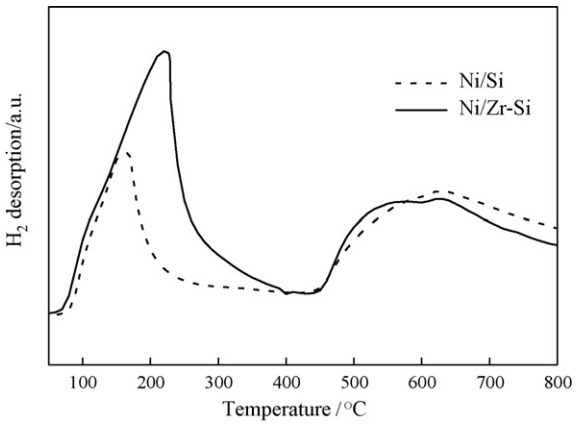

Fig. 6. H_2-TPD profiles of the Ni/Si and Ni/Zr–Si catalysts.

The surface acidity of ZrO_2–SiO_2 mixed oxide has been studied intensively by several groups [22–25]. It is widely accepted that the presence of ZrO_2 increase the amount of acid centers on ZrO_2–SiO_2 mixed oxide due to the formation of Si–O–Zr bond, which has been confirmed by the FT-IR characterization. Damyanova et al. [22] have studied the acid promotion mechanism of ZrO_2 with XPS and FT-IR. They supposed that the ZrO_2 was responsible for Lewis acidity in ZrO_2/SiO_2 mixed oxide due to the higher ionicity of the Zr–O bond, and Bronsted acid sites are produced because of the reduction of the electron density of the O–H bond, which caused by the Zr–O higher ionicity bonds neighboring the more covalent Si–O units. Anderson et al. [23] have especially studied the surface acidity of silica–zirconia aerogel with different Si/Zr ratios. They also proved that the Lewis acid sites originated from ZrO_2 and a roughly linear increased in Lewis acid density as a function of mol% ZrO_2 is expectable. Apparently, NH_3-TPD results suggest that the formation of Si–O–Zr bond due to the addition of ZrO_2 promoter results in stronger acid strength and an increase in total amounts of acid of the ZrO_2–SiO_2 support.

The TPR profiles of the catalysts are shown in Fig. 5. The effect of ZrO_2 promoter on the reduction of NiO species is clearly shown by the changes of the TPR profile. The TPR profile of the Ni/Si catalyst shows a three-stage reduction, and a intense low-temperature peak, observed in the range of 330–450 °C with a T_{max} at around 360 °C, is attributed to the reduction of NiO species interacting weakly with support. The others are two high-temperature shoulder peaks in the range of 450–650 °C, attributed to the reduction of NiO species interacting strongly with support. The TPR profile of the Ni/Zr–Si catalyst also shows a three-stage reduction in the range of 330–700 °C. However, it is observed that the low-temperature reduction peak shifts slightly to higher temperature with a T_{max} at around 396 °C, which is in accord with the literature [26], indicating stronger interaction of NiO species with support. As is known, acid strength, number of acid sites and acid distribution of support can affect the adsorption of metal, the interaction between metal and support and the dispersion of metal on the support. Combined with the NH_3-TPD results, it can be concluded that the increase of the interaction between NiO species and ZrO_2–SiO_2 support is caused by stronger acid strength and larger amounts of acid of the ZrO_2–SiO_2 support.

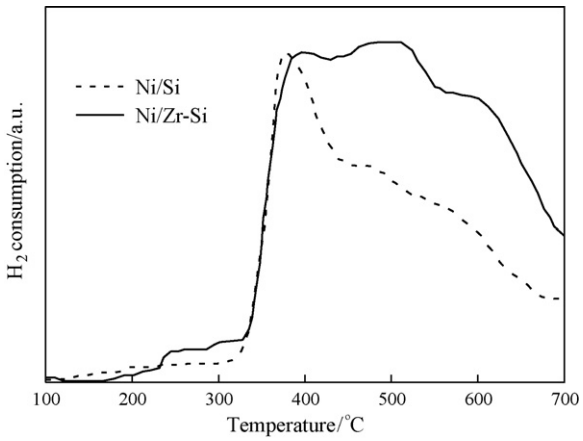

Fig. 5. TPR profiles of the Ni/Si and Ni/Zr–Si catalysts.

In addition, the dispersion of active metal on support is strongly influenced by metal-support interaction. Combined with the results of XRD and TEM, it can be seen that the appropriate interaction between NiO species with ZrO_2–SiO_2 support increases the dispersion degree of NiO species, and thus makes Ni crystallite size decrease after reduction. In Fig. 5, the total peak area of the Ni/Zr–Si catalyst has a progressive increase due to the addition of ZrO_2 promoter, indicating that NiO species has a higher reduction degree. Therefore, it is concluded that the Ni/Zr–Si catalyst possesses higher Ni dispersion and more active Ni species after reduction, which is generally consistent with the results of H_2-TPD (will be presented shortly).

The H_2-TPD profiles of the catalysts are shown in Fig. 6. From Fig. 6, it can be seen that the profiles exhibit two peaks in lower temperature (<400 °C) and higher temperature (>400 °C) ranges, respectively. The lower temperature peak corresponds to the desorption of H_2 which is weakly adsorbed on the metal surface. The higher temperature peak located at *ca.* 600 °C could be originated from strongly chemisorbed H_2. Compared with the Ni/Si catalyst, the temperature and the peak area of the higher temperature peak has little or no difference, but the lower temperature peak shifts to a higher temperature and the peak area becomes larger for the Ni/Zr–Si catalyst, suggesting that it possesses stronger adsorption ability for H_2 and more active Ni species. The Ni dispersion of the Ni/SiO_2 and Ni/ZrO_2–SiO_2 estimated from the amount of desorbed H_2 are 10.6% and 12.8%, respectively. The results are consistent with the conclusion of H_2-TPR.

3.2. The catalytic activity for CO methanation

The catalytic activities of the catalysts for CO methanation as a function of temperature are shown in Fig. 7. As seen from Fig. 7, the CO methanation occurs at the initial temperature of 120 °C on the both catalysts. In the temperature range of 160–220 °C, CO conversion shows an evident upward trend with the increase of reaction temperature, but at the same temperature CO conversion on the

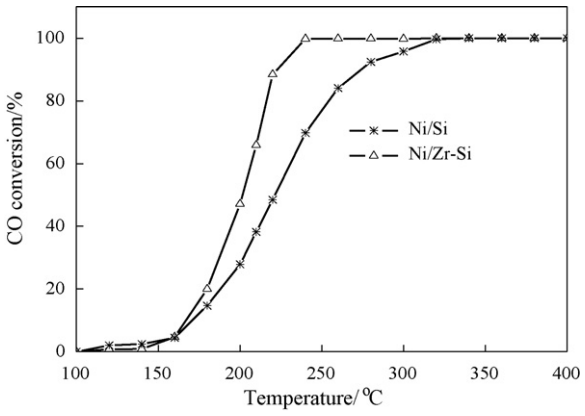

Fig. 7. Effect of reaction temperature on the catalytic activities of the catalysts.

Ni/Zr–Si catalyst is higher than that on the Ni/Si catalyst. CO can be completely transformed into CH_4 on the Ni/Zr–Si catalyst at 240 °C, but not completely transformed until the temperature was raised to 320 °C on the Ni/Si catalyst under the same reaction conditions. Apparently, the addition of ZrO_2 promoter improves remarkably the catalytic activity of the Ni/Zr–Si catalyst for CO methanation.

As seen clearly from the results of FT-IR and NH_3-TPD, the Si–O–Zr bond is formed due to the addition of ZrO_2 promoter, and the ZrO_2–SiO_2 support possesses stronger acid strength and larger amounts of acid due to the formation of the Si–O–Zr bond. The acidity changes lead to an increase of the interaction between NiO species and the ZrO_2–SiO_2 support. XRD, TEM, H_2-TPR and H_2-TPD results suggest the appropriate interaction enhances the dispersion degree and the reduction degree of NiO species on ZrO_2–SiO_2 support. Of course, the factors ultimately lead to the decrease of Ni crystallite size, the increase of the Ni dispersion and the number of active Ni species, and the enhancement of its adsorption ability for H_2. So we can conclude that smaller Ni crystallite size, higher Ni dispersion, more active Ni species and stronger adsorption ability for H_2 may contribute to higher catalytic activity of the Ni/ZrO_2–SiO_2 catalyst for CO methanation.

4. Conclusions

The Ni/SiO_2 and Ni/ZrO_2–SiO_2 catalysts were prepared by the impregnation method and the effect of ZrO_2 promoter on the structure and catalytic activity of the Ni/SiO_2 catalyst had been investigated. The tests for CO methanation indicate that the Ni/ZrO_2–SiO_2 catalyst shows higher catalytic activity than the Ni/SiO_2 catalyst. The results of characterization reveal that the addition of ZrO_2 promoter results in stronger acid strength and larger amounts of acid of the ZrO_2–SiO_2 support, and thus lead to an increase of the interaction between NiO species and ZrO_2–SiO_2 support. The appropriate interaction makes NiO species possess a higher dispersion degree and reduction degree, thus the Ni/ZrO_2–SiO_2 catalyst possesses smaller Ni crystallite size, higher Ni dispersion, more active Ni species and stronger adsorption ability for H_2, which may contribute to higher catalytic activity for CO methanation.

Acknowledgements

This work is supported by the Scientific and Technological Project of Shanxi Province (20080321017) and the National High Technology Research and Development Program of China (863 Program, 2005AA001050) and the National Natural Science Foundation of China (20573071).

References

[1] D.L. Trimm, Z.I. Onsan, Onboard fuel conversion for hydrogen-fuel-cell-driven vehicles, Catal. Rev. 43 (2001) 31–48.
[2] Q.H. Liu, X.F. Dong, X.M. Mo, W.M. Lin, Selective catalytic methanation of CO in hydrogen-rich gases over Ni/ZrO_2 catalyst, J. Nat. Gas Chem. 17 (2008) 268–272.
[3] C. Wu, H.M. Zhang, B.L. Yi, Hydrogen generation from catalytic hydrolysis of sodium borohydride for proton exchange membrane fuel cells, Catal. Today 93–95 (2004) 477–483.
[4] F. Joensen, J.R. Rostrup-Nielsen, Conversion of hydrocarbons and alcohols for fuel cells, J. Power Sources 105 (2002) 195–201.
[5] S. Takenaka, T. Shimizu, K. Otsuka, Complete removal of carbon monoxide in hydrogen-rich gas stream through methanation over supported metal catalysts, Int. J. Hydrogen Energy 29 (2004) 1065–1073.
[6] D.L. Trimm, Minimisation of carbon monoxide in a hydrogen stream for fuel cell application, Appl. Catal. A: Gen. 296 (2005) 1–11.
[7] K. Yaccato, R. Carhart, A. Hagemeyer, A. Lesik, P. Strasser, A.F. Volpe, H. Turner, H. Weinberg, R.K. Grasselli, C. Brooks, Competitive CO and CO_2 methanation over supported noble metal catalysts in high throughput scanning mass spectrometer, Appl. Catal. A: Gen. 296 (2005) 30–48.
[8] A.L. Kustov, A.M. Frey, K.E. Larsen, T. Johannessen, J.K. Nørskov, C.H. Christensen, CO methanation over supported bimetallic Ni–Fe catalysts: from computational studies towards catalyst optimization, Appl. Catal. A: Gen. 320 (2007) 98–104.
[9] Y.C. Lin, K.L. Hohn, Effect of sol–gel synthesis on physical and chemical properties of V/SiO_2 and V/MgO catalysts, Catal. Lett. 107 (2006) 215–222.
[10] M.L. Kantam, B.P.C. Rao, R.S. Reddy, N.S. Sekhar, B. Sreedhar, B.M. Choudary, Aerobic epoxidation of olefins catalyzed by Co–SiO_2 nanocomposites, J. Mol. Catal. A: Chem. 272 (2007) 1–5.
[11] Y.X. Zhao, X.Q. Qin, Z.G. Wu, L.P. Xu, D.S. Liu, Comparison of NiO–SiO_2, NiO–Al_2O_3 and NiO–Al_2O_3–SiO_2 catalysts for selective hydrogenation of maleic anhydride, J. Fuel Chem. Technol. 31 (2003) 263–266.
[12] Y.X. Zhao, Z.G. Wu, L.Q. Zhang, D.S. Liu, X.L. Xu, Study on the selective hydrogenation of maleic anhydride over ultrafine NiO/SiO_2 catalyst, J. Mol. Catal. (China) 16 (2002) 55–59.
[13] Y.F. Li, X.F. Dong, W.M. Lin, Effects of ZrO_2-promoter on catalytic performance of CuZnAlO catalysts for production of hydrogen by steam reforming of methanol, Int. J. Hydrogen Energy 29 (2004) 1617–1621.
[14] W. Zhou, K.G. Fang, J.G. Chen, Y.H. Sun, Effect of ZrO_2 on the stability of Co/SiO_2 catalyst for Fischer–Tropsch synthesis, J. Fuel Chem. Technol. 34 (2006) 461–465.
[15] M.S. Rana, S.K. Maity, J. Ancheyta, G.M. Dhar, T.S.R. Prao, MoCo (Ni)/ZrO_2–SiO_2 hydrotreating catalysts: physico-chemical characterization and activities studies, Appl. Catal. A: Gen. 268 (2004) 89–97.
[16] C.G. Gao, Y.X. Zhao, D.S. Liu, Liquid phase hydrogenation of maleic anhydride over nickel catalyst supported on ZrO_2–SiO_2 composite aerogels, Catal. Lett. 118 (2007) 50–54.
[17] J.I. Langford, A.J.C. Wilson, Scherrer after sixty years: a survey and some new results in the determination of crystallite size, J. Appl. Crystallogr. 11 (1978) 102–113.
[18] K. Kamiya, T. Yoko, K. Tanaka, M. Takeuchi, Thermal evolution of gels derived from $CH_3Si(OC_2H_5)_3$ by the sol–gel method, J. Non-Cryst. Solids 121 (1990) 182–187.
[19] Z.Q. Zhan, H.C. Zeng, A catalyst-free approach for sol–gel synthesis of highly mixed ZrO_2–SiO_2 oxides, J. Non-Cryst. Solids 243 (1999) 26–38.
[20] S.W. Lee, R.A. Condrate Sr., The infrared and Raman spectra of ZrO_2–SiO_2 glasses prepared by a sol–gel process, J. Mater. Sci. 23 (1988) 2951–2959.
[21] J.B. Miller, E.I. Ko, Control of mixed oxide textural and acidic properties by the sol–gel method, Catal. Today 35 (1997) 269–292.
[22] S. Damyanova, P. Grange, B. Delmon, Surface characterization of zirconia-coated alumina and silica carriers, J. Catal. 168 (1997) 421–430.
[23] J.A. Anderson, C. Fergusson, I. Rodifguez-Ramos, A. Guerrero-Ruiz, Influence of Si/Zr ratio on the formation of surface acidity in silica–zirconia aerogels, J. Catal. 192 (2000) 344–354.
[24] S. Damyanova, L. Petrov, M.A. Centeno, P. Grange, Characterization of molybdenum hydrodesulfurization catalysts supported on ZrO_2–Al_2O_3 and ZrO_2–SiO_2 carriers, Appl. Catal. A: Gen. 224 (2002) 271–284.
[25] C. Flego, L. Carluccio, C. Rizzo, C. Perego, Synthesis of mesoporous SiO_2–ZrO_2 mixed oxides by sol–gel method, Catal. Commun. 2 (2001) 43–48.
[26] R. Takahashi, S. Sato, T. Sodesawa, M. Yoshida, S. Tomiyama, Addition of zirconia in Ni/SiO_2 catalyst for improvement of steam resistance, Appl. Catal. A: Gen. 273 (2004) 211–215.